

Calculating the nuclear mass at finite angular momenta

B.G. Carlsson and I. Ragnarsson

Division of Mathematical Physics, Lund Institute of Technology, P.O. Box 118, SE-221 00 Lund, Sweden

Mean field methods to calculate the nuclear mass are extended into the high-spin regime to calculate the nuclear binding energy as a function of proton number, neutron number and angular momentum. Comparing the trend as a function of mass number for a selection of high-spin states, a similar agreement between theory and experiment is obtained as for ground state masses.

PACS numbers: 21.10.-k, 21.10.Dr, 21.60.-n, 21.60.Ev

A fundamental property of nuclei is their mass or equivalently, their binding energies, \mathcal{B} . The variation of the nuclear mass with proton and neutron number will reveal the shell effects which are closely related to the magic numbers and the extra binding associated with these numbers. It will also give some general idea about which regions of nuclei are deformed and if some specific particle numbers gives rise to extra binding for deformed nuclear shapes. In recent years, it has become possible to study a large number of nuclei up to very high angular momenta. A natural extension is then to study the variation of the total nuclear energy as a function of the angular momentum, I , i.e. to extend the investigations of the binding energy to three dimensions, $\mathcal{B}(Z, N, I)$.

A first attempt to study the experimental shell effects at high spin was carried out in Ref. [1] where the energies of high-spin states in $Z = 50-82$ nuclei were plotted relative to a somewhat schematic rotating liquid drop energy. In the present study we will instead investigate how well the high-spin states in a few selected nuclei are reproduced by state-of-the-art macroscopic-microscopic calculations. A big simplification at high spin is that pairing correlations are negligible which should make our calculations more reliable. We will thus consider a limited number of nuclei whose level schemes are known up into the unpaired regime and which have been successfully interpreted in calculations.

In the present study, we will start from the finite range version of the liquid drop model because for this model systematic fits to the masses of all nuclei with $N, Z \geq 8$ have been performed [2]. It turns out however that this model has some problems at low mass numbers where the energy becomes unstable with respect to high multipole deformations [3]. Therefore, we will also consider a recent version of a classical liquid drop formula, the LSD model [4] where an $A^{1/3}$ curvature term has been added to the classical Myers-Swiatecki expressions [5].

In the macroscopic-microscopic approach, the total nuclear energy is obtained as

$$E_{\text{tot}} = \min_{def} \left[E_{\text{l.d.}}(def) + \frac{\hbar^2 I(I+1)}{2\mathcal{J}_{\text{rig.}}(def)} + E_{\text{shell}}(def, I) \right] \quad (1)$$

in the high-spin limit when pairing is ignored. In the formula, it has been specified which terms depend on deformation (def) and angular momentum, I , respectively. The two first terms correspond to the rotating liquid drop

energy and the third term is the shell energy.

In order to calculate the shell effects at high spin, we will rely on cranked Nilsson-Strutinsky (CNS) formalism with the modified oscillator potential because it is only in this model [6, 7] that systematic high-spin calculations have been carried out for nuclei in essentially all mass regions. In order to keep the number of parameters as small as possible, we have used the so-called $A = 110$ parameters [7] for all nuclei. These parameters have been optimized for nuclei with $A = 100 - 150$ but should be approximately applicable for all mass numbers.

As one alternative for the static liquid drop energy, $E_{\text{l.d.}}$ in Eq. (1), we consider the finite range liquid drop model (FRLDM) [2] which is more consistent [8] than the finite range droplet model (FRDM) in the description of fission and thus probably more reliable for strongly deformed shapes. The FRLDM parameters have been fitted to reproduce ground state masses for 1654 nuclei and 28 fission-barrier heights. The resulting root mean square error after experimental errors have been compensated for is $\sigma_{\text{th}} = 0.779$ MeV [2]. In the present study, this model can not be applied directly because pairing is important at the ground state while we are interested in unpaired high-spin states. Indeed, in the fit, an average pairing energy is included in the macroscopic liquid drop energy and must be removed. Furthermore, a zero-point energy for vibrations in the elongation direction is also included which appears inconsistent for high-spins where the special symmetry favoring axial shapes is broken. One might consider to include the full quadrupole zero-point energy term but this would be very difficult in practice. Thus, a new fit to the same masses has been performed where the full pairing interaction has been included in the microscopic terms and where no zero-point energy is included. This new fit gives a very similar mean square error, namely $\sigma_{\text{th}} = 0.778$ MeV, corresponding to a ‘standard’ root mean square error of 0.783 MeV. The biggest difference between the two fits is the constant term which increases from 2.6 to 7.2 MeV but there are also minor differences in all other terms.

The second alternative for the static liquid drop energy, the LSD model [4], has been fitted to the same shell corrections as the FRLDM for $Z \geq 29$ and $N \geq 29$ but for lighter nuclei semi-empirical shell corrections are used instead. Therefore, as illustrated for nuclei along β -stability in Fig. 1, the two models give very similar

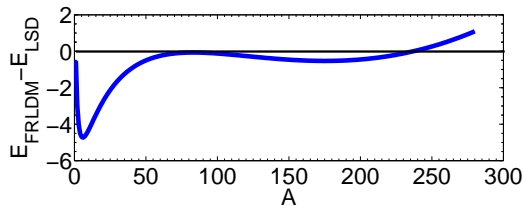


Figure 1: Difference in energy between the FRLDM and the LSD model for nuclei along the beta-stability line at spin zero and spherical shape.

energies for mass numbers $A \approx 50 - 250$ but they become rather different for smaller mass numbers. The LSD model has been fitted to 2766 masses with a root mean square error of 0.698 MeV which decreases to 0.610 MeV when only 1654 masses are considered. In order to remove the zero-point energy and the average pairing when using the LSD model without refitting the parameters we make an estimate based on the two fits for the FRLDM. We calculate the energy difference for a spherical nuclei between the two fits and add this contribution to the LSD model. This way we introduce a constant shift for each nucleus but we do not change the original deformation dependence in the model.

With the static liquid-drop energy fixed, it only remains to fix the parameters of the rigid moment of inertia which enters in the second term of Eq. (1). It can be calculated as [9]

$$\mathcal{J}_{\text{rig.}} = \frac{2}{5} M r_0^2 A^{2/3} \delta_{\mathcal{J}}(\varepsilon_2, \gamma, \varepsilon_4) + 4 M a^2 \quad (2)$$

where the radius for a spherical nucleus is parameterized as $r_0 A^{1/3}$ and where the diffuseness is introduced in the form of a Yukawa folding function with range a . A density distribution which changes from 10% to 90% of its central value in a distance of 2.4 fm is described by $a \approx 0.75$ fm. M is the nuclear mass which varies as A . The first expression on the right in Eq. (2) is the rigid body moment of inertia for a spherical nucleus with a sharp boundary. The deformation correction, $\delta_{\mathcal{J}}(\varepsilon_2, \gamma, \varepsilon_4)$, which equals one for spherical shape, is larger than one for shapes mainly relevant for rapidly rotating nuclei, i.e. for rotation around the smaller axis ($0^\circ < \gamma < 60^\circ$). Note that the diffuseness correction (the last term in Eq. 2) is independent of deformation.

The moment of inertia parameters, r_0 and a are obtained by a fit to experimentally determined nuclear charge density distributions. We fit the root-mean-square value of the radius $\langle r^2 \rangle^{1/2}(\varepsilon_2, r_0, a)$, calculated with a Yukawa folding function, to the values given in Ref. [10] for 116 nuclei with $A > 16$. The quadrupole deformations of the ground-states are taken from Ref. [2]. The result of the fit is $r_0 = 1.1599$ fm and $a = 0.5984$ fm and the standard deviation of the errors are $s = 0.0454$ fm. Since the root-mean-square radius as well as the moment of inertia involves integrals over $\langle x^2 \rangle$, $\langle y^2 \rangle$ and $\langle z^2 \rangle$,

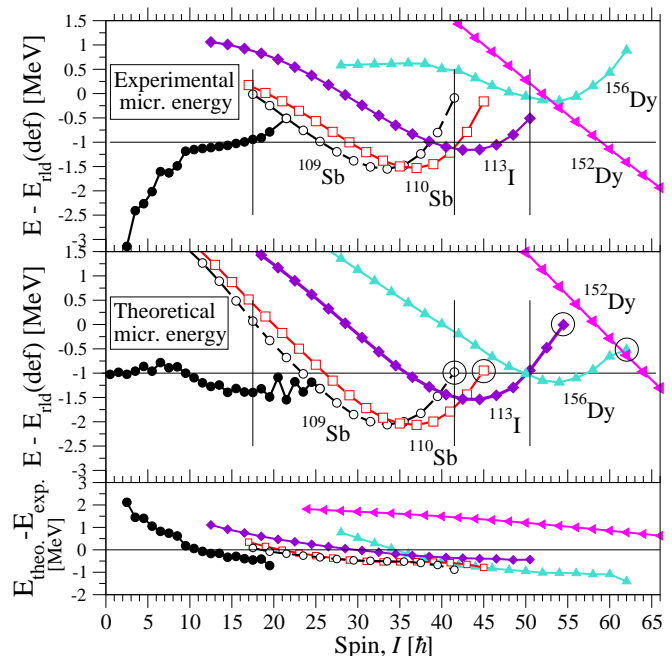


Figure 2: Experimental (top panel) and theoretical (middle panel) microscopic energies and their difference (lower panel) for some well-established high-spin bands in $A = 109 - 156$ with the level scheme of ^{109}Sb extended down to $I = 0$. The LSD model and a diffuse surface ($r_0=1.16$ fm, $a=0.6$ fm) has been used when calculating the first and second terms, respectively, of Eq. (1). Calculated states where all valence nucleons have their spin vectors aligned with the axis of rotation (terminating states) are circled.

this should give accurate values for the moment of inertia even though there might be a larger uncertainty in the two values, r_0 and a .

Fig. 2 illustrates the total energy for a few nuclei as a function of spin. It is drawn using the LSD model for the static liquid drop energies and radius constants $r_0=1.16$ fm and $a=0.6$ fm obtained from the fit described above. For each nucleus the energy of the corresponding rotating liquid drop has been subtracted. This is thus a straightforward generalization of ‘standard’ mass plots, see e.g. Figs. 1 and 2 of Ref. [2], which gives us a convenient scaling when comparing the microscopic energy for different nuclei or when comparing theory and experiment.

The yrast line for ^{109}Sb in Fig. 2 is drawn starting from low spins where the discrepancies between between calculations and experiment should be an approximate measure of the pairing energy which is not included in the calculations. The high-spin bands in $^{109,110}\text{Sb}$ are both observed to terminate at $I = 41.5$ and $I = 45$, respectively. They are some of the first and best developed smooth terminating bands in the $A = 110$ region [7]. Relative to the ^{100}Sn core, they have two proton holes in the $g_{9/2}$ shell and one proton and two and three neutrons, respectively, in the high- j $h_{11/2}$ orbitals. The band in ^{113}I , referred to as band 1 in Ref. [11], has the

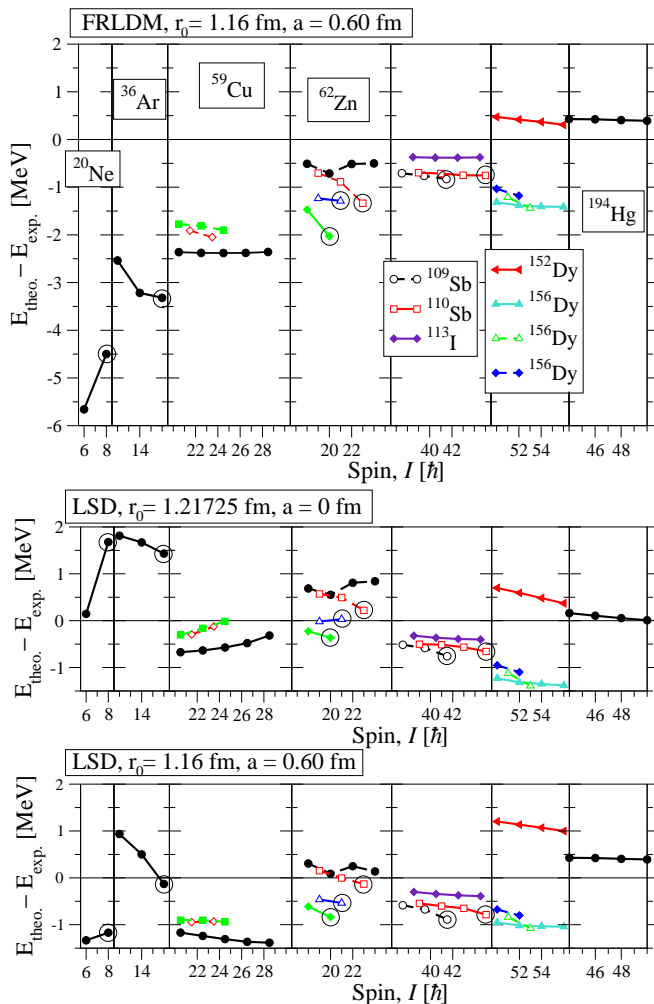


Figure 3: Difference in total energy between theory and experiment for 10 nuclei with masses in the range $A = 20 - 194$. In the lower panel, the same parameters as in Fig. 2 have been used while in the upper panel, the LSD model for the static liquid drop energy has been replaced by the FRLDM and, in the middle panel the diffuse surface when calculating the rigid moment of inertia has been replaced by a sharp surface.

same number of holes and thus more valence particles which means that it has a higher terminating spin value at $I^\pi = 54.5^+$ and it is observed up to $I = 50.5$. The ^{156}Dy band [12] shown in Fig. 2 is yrast at the highest spin values. It is interpreted as having four proton holes in the $Z = 64$ core and is tentatively observed to its termination at $I = 62$. The band drawn for ^{152}Dy is the first superdeformed band identified [13] in the $A = 150$ region and the only such band whose absolute excitation energy is known [14]. Its interpretation in CNS calculations is discussed in Ref. [15].

In order to extend the comparison of Fig. 2 to a larger mass region, we compare calculated and experimental energies for additional nuclei in Fig. 3 where different versions of the rotating liquid drop formula are used. Before discussing the details of this figure, we will briefly de-

scribe the rotational bands which in addition to the ones previously discussed have been included in the comparison. The band observed to terminate at 8^+ in $^{20}\text{Ne}_{10}$ [16] is built with two valence protons and two valence neutrons in the $d_{5/2}$ shell. Cranked Nilsson-Strutinsky calculations for this band have been discussed e.g. in Ref. [17] and reviewed in [7]. The band in ^{36}Ar is the so called superdeformed band which is interpreted in CNS as well as shell model calculations as having identical proton and neutron configurations with two particles in $f_{7/2}$ and two holes in $p_{3/2}$ [18]. The highest spin band shown for ^{59}Cu [19] has been referred to as superdeformed with four holes in the ^{56}Ni core and consequently seven particles in open shells with three of them in high- j $g_{9/2}$ orbitals. The other band (with both signatures shown) has three holes and two of the six particles in $g_{9/2}$ orbitals. The two bands in ^{62}Zn have one hole in the core and two or three of the seven valence particles in the $g_{9/2}$ shell [20]. For ^{156}Dy , the two negative parity bands observed to highest spin, $I^\pi = 52^-, 53^-$ are included in addition to the band shown in Fig. 2. Of the three superdeformed bands linked to the normal-deformed states in the $A = 190$ region, the band in ^{194}Hg [21] has been included in our comparison because it is observed to higher spins than the other bands. According to the present calculations, it has the high- j $\pi(i_{13/2})^4\nu(j_{15/2})^4$ configuration in agreement with standard interpretations, see e.g. [22].

With the same parameters used in Fig. 2 and in the lower panel of Fig. 3, those data points that are repeated are identical. These parameters describe the data with good accuracy. Typical errors are in the range of ± 1 MeV. Note especially that from the limited data set considered here, the general trend as a function of mass number appear correct. This is contrary to the results in the upper panel where in the static liquid drop energy, the LSD model has been replaced by the FRLDM. This results in systematic differences for light nuclei where the calculated energies are lower than the experimental energies. Thus, the FRLDM predicts similar results as the LSD model for heavy nuclei but substantially lower total energies for ^{20}Ne , ^{36}Ar and ^{59}Cu . One reason for this is that the two models are fitted to different shell corrections for $Z < 29$ and $N < 29$ (as seen in Fig. 1). Another reason is that for light nuclei the two models have different deformation dependencies, with the FRLDM being softer in the ε_2 and ε_4 directions. Therefore for light nuclei the FRLDM generally predicts somewhat larger ε_2 deformations and in some cases so large ε_4 deformations that the corresponding shapes appear unrealistic. Consider for example the terminating state in ^{36}Ar which is predicted to have a deformation of $\varepsilon_2 = 0.415$ and $\varepsilon_4 = 0.188$ using the FRLDM and $\varepsilon_2 = 0.356$ and $\varepsilon_4 = 0.065$ in the LSD model. Similar results are obtained for the terminating state in ^{20}Ne which is predicted to have a deformation of $\varepsilon_2 = 0.120$ and $\varepsilon_4 = 0.210$ using the FRLDM and $\varepsilon_2 = 0.092$ and $\varepsilon_4 = 0.033$ in the LSD model.

The only difference between the two lower panels in

Fig. 3 is that a sharp surface is used when calculating the rigid body moment of inertia in the middle panel while a diffuse surface is used in the lower panel. The radius in the sharp surface case is chosen as the value used to calculate the Coulomb energy in the LSD formula, $r_0 = 1.21725$ fm corresponding to a rigid moment of inertia of a sphere which is about the same as in the diffuse surface case for $A \approx 140$. In general, the differences between the two lower panels are not so big for heavy nuclei but become more pronounced for light nuclei. For example, the ‘diffuse moment of inertia’ for spherical shape is around 13 % bigger for $A = 36$ and more than 20 % bigger for $A = 20$. For ^{20}Ne and ^{36}Ar , this results in an energy difference between 2.5 and 3 MeV for the terminating $I = 8$ and $I = 16$ states, respectively. For large deformations however, these differences become smaller because the diffuseness correction to the moment of inertia is independent of deformation (Eq. 2). Thus, for the strongly deformed 16^+ state in ^{36}Ar , the difference is only about 1.5 MeV in the full calculation while for the less deformed 8^+ state of ^{20}Ne its around 3 MeV. Differences up to about 1 MeV are then seen in the bands for the $A = 60$ nuclei. An interesting effect is seen in the superdeformed band in ^{152}Dy . For spherical shape, the two formula for the moment of inertia give energy differences (in opposite direction relative to the light nuclei) of only around 0.2 MeV for $I = 60$ but the difference increases to 0.7 MeV at the calculated 2:1 deformation of the superdeformed band.

With the present formalism we are thus able to put experimental and theoretical results on a common absolute scale for high-spin calculations with no pairing. In previous calculations, either the nuclear binding energy at the ground state has been considered as a function of N and Z or the energy of a specific nucleus has been considered as a function of angular momentum, I . Systematic trends or variations of the microscopic energy at high spin might provide us with new insight into high-spin phenomena, for example making it possible to compare regions where angular momentum is built mainly from collective rotation and mainly from single-particle excitations, re-

spectively. A different aspect is that the prediction of prompt particle decay from high-spin states, which has been observed [23] for example in the nucleus ^{59}Cu discussed here, requires reliable estimates of the absolute energy difference between the mother and daughter nucleus.

A natural extension of the present approach is to include many more nuclei to see if the general trends of Fig. 3 are still the same. One could also make a new mass fit in the high-spin region varying r_0 and a in the moment of inertia formula or in the long run, adjust ‘all parameters’ in a global fit in the N, Z, I space in which case it would clearly be necessary to also include pairing. One possibility might be to calculate the pairing energy only for $I = 0$ and postulate a semiempirical formula how it slowly disappears with angular momentum in which case it would be possible to keep the configuration tracing in the high-spin regime which is one of the most important features of the CNS approach. Especially for light nuclei, the high-spin data appears important. For example, it might be possible to obtain a more reliable estimate of the stiffness towards deformation for nuclei with $A \lesssim 100$ where fission barrier data are unknown or uncertain but where the energy of several strongly deformed high-spin bands are well established.

In summary, a consistent recipe has been introduced to consider the total energy in the full N, Z, I space. Good agreement between calculations and experiment is obtained using a standard liquid drop expression with an $A^{1/3}$ curvature term, an average moment of inertia calculated from a diffuse surface mass distribution and shell corrections based on the modified oscillator potential. For high-spin states in the mass range $A = 20 - 200$, the discrepancies appear comparable to those obtained in state of the art mass calculations. The consequences of using different models when calculating the rotating liquid drop energy were investigated.

The authors would like to thank Peter Möller for fitting the parameters of the FRLDM. This work was supported by the Swedish Science Research Council.

-
- [1] I. Ragnarsson *et al.*, Int. J. Mod. Phys. **E 13**, 87 (2004).
 - [2] P.Möller *et al.*, At. Data Nucl. Data Tables **59**, 185 (1995)
 - [3] L-O. Jönsson, Nucl. Phys. **A608**, 1 (1996).
 - [4] K. Pomorski and J. Dudek, Phys. Rev. C **67**, 044316 (2003)
 - [5] W.D. Myers, W.J. Swiatecki, Nucl. Phys. **A81** (1966) 1
 - [6] T. Bengtsson and I. Ragnarsson, Nucl. Phys. **A436**, 14 (1985).
 - [7] A.V. Afanasjev *et al.*, Phys. Rep. **322**, 1 (1999).
 - [8] P. Möller, A.J. Sierk and A. Iwamoto, Phys. Rev. Lett. **92**, 072501 (2004).
 - [9] K.T.R. Davies and J.R. Nix, Phys. Rev. **C14**, 1977 (1976).
 - [10] H. De Vries, C.W. De Jager and C. De Vries, At. Data Nucl. Data Tables **36**, 495 (1987)
 - [11] K. Starosta *et al.*, Phys. Rev. C **64** 014304 (2001).
 - [12] F. G. Kondev *et al.*, Phys. Lett. B **437** 35 (1998).
 - [13] P. Twin *et al.*, Phys. Rev. Lett. **57**, 811 (1986).
 - [14] T. Lauritsen *et al.*, Phys. Rev. Lett. **89**, 282501 (2002).
 - [15] I. Ragnarsson, Nucl. Phys. **A557**, 167c (1993).
 - [16] T. K. Alexander *et al.*, Nucl. Phys. **A179**, 477 (1972).
 - [17] I. Ragnarsson, S. Åberg and R. K. Sheline, Physica Scripta **24** (1981) 215.
 - [18] C.E. Svensson *et al.*, Phys. Rev. Lett. **85**, 2693 (2000).
 - [19] C. Andreoiu *et al.*, Eur. Phys. J. **A14**, 317 (2002).
 - [20] C. E. Svensson *et al.*, Phys. Rev. Lett. **80**, 2558 (1998).
 - [21] T.L. Khoo *et al.*, Phys. Rev. Lett. **76**, 1583 (1996).
 - [22] W. Satula *et al.*, Nucl. Phys. **A529**, 289 (1991).
 - [23] D. Rudolph *et al.*, Phys. Rev. Lett. **89**, 022501 (2002).